POLITECNICO DI TORINO
Repository ISTITUZIONALE

Relating physical properties to temperature-induced damage in carbonate rocks

Original
Relating physical properties to temperature-induced damage in carbonate rocks / Vagnon, Federico; Colombero, Chiara; Comina, Cesare; Ferrero, Anna Maria; Mandrone, Giuseppe; Missagia, R; Vinciguerra, Sergio Carmelo. - In: GÉOTECHNIQUE LETTERS. - ISSN 2045-2543. - 11:2(2021), pp. 1-11. [10.1680/jgele.20.00122]

Availability:
This version is available at: 11583/2909454 since: 2022-03-24T21:12:44Z

Publisher:
ICE Publishing

Published
DOI:10.1680/jgele.20.00122

Terms of use:

This article is made available under terms and conditions as specified in the corresponding bibliographic description in the repository

Publisher copyright

(Article begins on next page)

20 March 2024

Relating physical properties to temperature induced damage in carbonate rocks.

Dr. **Federico Vagnon**, Department of Earth Sciences, Università di Torino, Torino, 10125, Italy, orcid: 0000-0003-0539-0557

Dr. **Chiara Colombero**, Department of Environment, Land and Infrastructure Engineering, Politecnico di Torino, Torino, 10129, Italy, orcid: 0000-0001-9818-7464

Prof. **Cesare Comina**, Department of Earth Sciences, Università di Torino, Torino, 10125, Italy, orcid: 0000-0002-3536-9890

Prof. **Anna Maria Ferrero**, Department of Earth Sciences, Università di Torino, Torino, 10125, Italy, orcid: 0000-0001-8422-6303

Prof. **Giuseppe Mandrone**, Interuniversity Department of Regional and Urban Studies and Planning, Torino, 10125, Italy, orcid: 0000-0002-5397-9377

Prof. **Roseane Missagia**, Universidade Estadual Norte Fluminense - Darcy Ribeiro/UENF, Laboratorio de Engenharia e Exploração de Petroleo/LENEP, 27925-535 Macaé – RJ – Brasil, orcid: 0000-0001-6284-6755

Prof. **Sergio Carmelo Vinciguerra,** Department of Earth Sciences, Università di Torino, Torino, 10125, Italy, orcid: 0000-0002-6939-3549

Correspondence to: Federico Vagnon, federico.vagnon@unito.it

Words: 1953 - Figures: 8 - Tables: 4

Abstract

Carbonate rocks have a widespread diffusion in the Earth crust and are extensively used in cultural heritage and buildings. These rocks can be naturally or anthropically exposed to high temperatures. Consequently, relating physical properties to temperature induced damage is extremely important. Six sets of compositionally and texturally different carbonate rocks, spanning from limestones and marbles to dolomitic marbles, were analysed in this study. Different physical properties, such as porosity, seismic wave velocities and electrical resistivity, were measured before and after thermal treatments with heating/cooling ranges between 105°C and 600°C. Microscopic observations and optical analyses were used to investigate how the temperature induced damage influences the physical measured properties of the different microstructures. This integrated approach allowed to define a relationship between physical properties and thermal induced damage, via an induced damage index valid for a broad suite of carbonate rocks.

Key words

Carbonate rocks; thermal treatment; physical properties; thermal damage factor.

List of notations:

c	fitting parameter, depending on the specific rock structure and rock degradation effect
CU	uniformity coefficient
D	damn index
D10	value of the grain diameter at 10% of the cumulative distribution
D50	value of the grain diameter at 50% of the cumulative distribution
D60	value of the grain diameter at 60% of the cumulative distribution
ER	electrical resistivity
F	formation factor
n	porosity
P(T)	physical parameter at temperature T
P_0	reference physical parameter value at 20°C
UPV	ultrasonic pulse velocity
VP	P-wave velocity
VS	S-wave velocity
$\rho_{a,WET}$	apparent resistivity in saturated condition
ρ_{fluid}	resistivity of the saturating fluid

1. Introduction

High temperature gradients drive mechanisms of degradation and weakening of rocks, thus controlling a number of geological processes, engineering applications and cultural heritage (Vagnon et al., 2019 and references there in).
Among various rocks, carbonates are widespread diffused and are extensively used in cultural heritage artefacts and buildings. Large crustal volumes of carbonate rocks are naturally exposed to significant temperature increases in areas with anomalous geothermal gradients. The exposure to high temperatures could also be related to engineering applications. Forecasting their physical evolution under temperature gradients is therefore of utmost importance for many fields of rock mechanics.
While numerous studies have investigated the damage mechanisms induced by temperature effects on carbonate rocks (Heap et al., 2013; Castagna et al., 2018 and reference there in), less attention has been paid to quantitatively generalize throughout physical parameters evolution the thermal degradation induced by heating.
A relationship linking physical parameters and temperature (thermal degradation relationship) has been proposed by several authors (e.g. Koca et al., 2006; Dwivedi et al., 2008; Zhao et al., 2012; Musso et al., 2015; Weydt et al. 2018; Vagnon et al., 2019) under the form:

$$P(T) = P_0 e^{\pm cT} \qquad (1)$$

where *P(T)* is a given physical parameter at temperature T, P_0 is its reference value at 20°C and c is a fitting parameter, depending on the specific rock structure and rock degradation effect. The sign of the exponent is positive if the considered parameter increases with temperature (negative otherwise). Based on experimental tests, several authors (Koca et al., 2006; Dwivedi et al., 2008; Zhao et al., 2012; Vagnon et al., 2019) have proposed similar exponential equations for the thermal degradation relationship.
This study has the main objective of defining a general relationship between physical properties and thermal induced damage, via a multiparametric induced damage index valid for a broad suite of carbonate rocks.
Six sets of different carbonate rock specimens were tested before and after thermal treatment, with heating/cooling cycles from 105°C to 600°C. Porosity, ultrasonic pulse velocity (UPV) and electrical resistivity (ER) were measured. Microstructural observations and both grain size distribution curves and crack densities were analysed. A unified multiparametric thermally induced damage coefficient was quantified to provide a general law for carbonate rocks.

2. Sample sets and experimental methods

Samples obtained from the four different sampling areas (Figure 1), were classified into six sets:

- 7 limestone samples, coming from the fossil hydrothermal system of Las Minas (Mexico), named “RLM” in the following;
- 10 dolomitic marble samples, coming from Granados Quarry (Tatatila, Mexico), named “GQ”;
- 11 marble samples, coming from San Lorenzo Quarry (Italy), named “VALDIERI”;
- 18 marble samples, coming from Italva Basin (Brazil), divided into three subsets (of 6 specimens respectively) and named “BRAZIL C”, “BRAZIL D” and “BRAZIL SJ”.

Differences in diameter were out of our control and merely linked to the instrumentation adopted at the sampling locations, but all the samples respected the geometric requirements for standard determination of the analyzed physical properties.

To check the chemical content of each set, X-ray fluorescence (XRF) and diffraction (XRD) analyses were performed (Table 1). From these analyses, it can be observed that RLM and VALDIERI samples are the mostly calcitic (97.3 and 98 % respectively) while GQ samples are essentially dolomitic. Brazilian samples show transitional compositions between these end members.
Following the experimental procedure detailed in Vagnon et al. (2019), porosity (n), P- and S-wave velocity (V_P and V_S) and electrical resistivity (in saturated conditions, $\rho_{a,WET}$) of the 46 core specimens were measured before and after heating (at target temperatures of 105, 200, 400 and 600°C respectively). Table 2 summarizes the measured parameters, the international standards and experimental methodologies adopted for their determination. The thermal treatment involved a three-stage procedure: i) sample heating up to the target temperature with a heating rate of 0.06°C/s; ii) 24-h sample exposure to constant target temperature; iii) slow-rate sample cooling down to room temperature (one day on average). The exposure time allows the uniform heating of the samples, ensuring that the surface temperature was the same inside the sample. Even in cooling phase, the time inside the furnace prevents thermal shocks that may influence the sample physical properties, by increasing the thermal degradation effects.
Values of $\rho_{a,WET}$ were also expressed in terms of formation factor, F (Archie, 1942), a dimensionless parameter that represents the ratio between $\rho_{a,WET}$ and the saturating fluid resistivity, ρ_{fluid}.
To analyze the main effects of thermal treatment on the micro-structure of the studied carbonate rocks, 20x40 mm thin sections were obtained from natural and thermal treated extra-samples belonging to the different sets. Microscopic observations were then performed using a transmitted polarized light microscope. By using the image processing program ImageJ (Schneider et al., 2012), the pre- and post-heating grain size distribution and crack length (Arganda-Carreras et al., 2010) were measured on thin sections. Crack density, expressed as the ratio between total cracks length and area investigated, was also proposed as a parameter for evaluating thermal damage.

3. Results

3.1 Physical parameter measurements

The thermal treatment induced significant changes in n, UPV and $\rho_{a,WET}$ values for each set of specimens. In Figure 2 all the data are shown. Exponential relationships were fitted to the different physical parameters for each data set.
Porosity (Figure 2a) showed an exponential trend with temperature for each set of specimens. In particular, the porosity of RLM limestones was more sensitive to temperature gradients than the other sets of tested specimens.
In general, all the sample sets exhibited the same trends of V_P and V_S with increasing target temperature (Figure 2b and 2c), but with initial P- and S-wave velocity values significantly different.
The formation factor values (F) of each individual set of rock samples is reported in Figure 2d. A clear modification in electrical properties is found between different rock samples, with increasing target temperature. In particular, F clearly decreased by increasing temperature.

3.2 Discussion and relationships between physical parameters

The previous section has highlighted a strong dependence of each single physical parameter on temperature, repeatable for all lithologies investigated. The main findings can be summarized as follows:

- The thermal treatment induced a moderate increase in porosity due to generation of new cracks or re-opening of existing ones at temperatures up to 550°C. At higher temperatures, the porosity increase was likely related to decalcination and decarbonation, leading to increased pore space because of the combination of grain comminution and crack damage (Heap et al., 2013). RLM samples showed a more marked increment in porosity compared to the other samples mirroring the fact that limestones undergo more pronounced textural changes, while marbles, already exposed to high temperatures in their formation history that has led to recrystallization, maintain a memory of the thermal stresses.
- The increase in porosity is mirrored by a decrease in P- and S-wave velocity and resistivity. With this respect VALDIERI samples showed a slightly different behaviour, since velocities remained relatively constant until 200°C with a significant increase only for higher temperatures. This can be correlated to the presence of dolomite that has been observed (Heap et al., 2013) to strengthen rocks at low temperatures, while decarbonation leads degradation at higher temperatures.
- Figure 3 and 4 show the inverse power law relationships between physical parameters and porosities. For the n-V_P and n-V_S relationships, the general degradation of physical parameters also influenced the mechanical characteristics of rock samples. For n-F relationship that represents the Archie's law, the determined parameters for the power law are not in agreement with typical observed values for carbonate rocks (e.g. Ara et al., 2001). However, the application of this relationship to carbonate rocks has been already recognized to be difficult due to the complexity of their voids space (e.g. Talabani et al., 2000).

3.5 Microstructural observations

Even if microphotographs of thin sections cannot be considered completely representative of the whole volume of the analyzed rock samples, their analysis can be very important for identifying how micromechanical damage induced by heating took place. In this respect, Figure 5 shows microphotographs of thin sections before (left column) and after thermal treatment (right column) at the highest temperature, i.e. 600°C, for all lithologies investigated. After heating at 600°C, grain expansion leading to crack generation along grain boundaries is observable in all the samples. Grain size analyses can be also considered as a good indicator of the thermal effects, given that the decalcination process can reduce the average grain size at high temperature (Heap et al. 2013). Moreover, the propagation of intragranular microcracks can have a double effect either on the crushing of existing grains or the increase in void volume. For these reasons, both grain size distributions (Figure 6) and crack length (Figure 7 and Table 4) of each microphotograph of Figure 5 were evaluated using the ImageJ code. Moreover, the values of the grain diameter at 50% of the cumulative distribution (D50), the uniformity coefficient (CU), obtained as the D60/D10 ratio and the crack density were additionally determined (Table 3 and Table 4).
The analyses highlighted that:

- the temperature increase generates a shift of the grain size distributions to smaller values, strengthening the hypothesis of the formation of microcracks inside initial bigger grains.
- RLM and VALDIERI samples experienced higher thermal degradation since they exhibit the highest increase in crack density. For RLM samples this is probably due to the fact that limestone underwent deeper textural changes with respect to metamorphic rocks or carbonates already affected by high temperature gradients and circulation of high temperature fluids.

4. Towards a unified damage index

From the above reported results, an induced damage index for carbonate rocks exposed to different temperatures can be proposed. For porosity, the induced damage index can be defined as:

$$D_n = 1 - \frac{n_{RT}}{n(T)} \quad (2)$$

where D_n is the induced damage index for porosity, n_{RT} is the room-temperature porosity and n(T) is the porosity evaluated at the different target temperature.
For the other parameters the induced damage index can be written:

$$D_{pP} = 1 - \frac{P(T)}{P_0} \quad (3)$$

where D_P is the induced damaged index for generic parameter.
The variation of damage index with temperature is shown in Figure 8 for each considered parameter. In general, damage indexes gradually increase with temperature following a logarithmic distribution. A dependence on the lithotype is also noticeable in terms of absolute values, while the relative trends remain comparable (Figure 8). The most plausible explanation may be found in the interplay of bulk composition and strength (dolomitization and/or grains recrystallisation) and degree of cementation.

Conclusion

A series of laboratory tests on six, compositionally and texturally different, carbonate rocks was performed to investigate the variation of multiple physical parameters as a function of increasing temperature.
The main findings of this study can be summarized as:

- In the range 200 to 400°C a turning point in the trend of physical behaviour is identified.
- The effect of temperature on physical properties depends mainly on rock texture, bulk composition and grain size distribution resulting from the interplay of the primary processes of rock formation and recrystallisation. In particular, if the rock was already naturally exposed to high temperatures, a stress memory is preserved and only minor changes in the physical parameters were detected after thermal treatment. As a consequence, limestone samples exhibit a much higher thermal damage compared to marbles already exposed at high temperature and circulation of fluids at high temperature, especially in term of porosity increase.
- An ubiquitous exponential relationship between physical parameter and temperature was found for each considered carbonate rock, where the exponent can have positive or negative sign:
  - c = 0.0053±0.003 for limestone;
  - c = 0.0038±0.0021 for fine grain marble;
  - c = 0.0026±0.0006 for coarse grain marble;
  - c = 0.0036±0.001 for dolomitic marble.
- A unified coefficient D for quantifying the thermal damage of rocks has been also proposed.

5. Conflicts of Interest

The authors declare that there is no conflict of interest regarding the publication of this paper.

Funding Statement

Part of the tests reported in this paper were funded by the European Union's Horizon 2020 research and innovation program under the grant agreement No. 727550.

References

Ara TS, Talabani S, Atlas B, Vaziri HH, Islam MR (2001) In-Depth Investigation of the Validity of the Archie Equation in Carbonate Rocks, in: Proceedings - SPE Production Operations Symposium. 177–183. https://doi.org/10.2523/67204-ms

Archie GE. (1942) The electrical resistivity log as an aid in determining some reservoir characteristics. Transactions of the American Institute of Mechanical Engineers, **146**, 54–67.

Arganda-Carreras I, Fernández-González R, Muñoz-Barrutia A, Ortiz-De-Solorzano C (2010) 3D reconstruction of histological sections: Application to mammary gland tissue. Microsc. Res. Tech. **73**, 1019–1029. https://doi.org/10.1002/jemt.20829

ASTM (2000) Laboratory Determination of Pulse Velocities and Ultrasonic Elastic Constants of Rock. Des. **D 2845 – 00 14**, 1–9.

Castagna A, Ougier-Simonin A, Benson PM, Browning J, Walker RJ, Fazio M, Vinciguerra S (2018) Thermal Damage and Pore Pressure Effects of the Brittle-Ductile Transition in Comiso Limestone. J. Geophys. Res. Solid Earth **123**, 7644–7660. https://doi.org/10.1029/2017JB015105

Dwivedi RD, Goel RK, Prasad VVR, Sinha A (2008) Thermo-mechanical properties of Indian and other granites. Int. J. Rock Mech. Min. Sci. **45**, 303–315. https://doi.org/10.1016/j.ijrmms.2007.05.008

Heap MJ, Mollo S, Vinciguerra S, Lavallée Y, Baud P, Dingwell DB, Iezzi G, von Aulock FW (2013) Thermal weakening of the carbonate basement under Mt. Etna volcano (Italy): Implications for volcano instability. J. Volc. Geother. Res. **250**, 42-60.

ISRM (1979) Suggested methods for determining water content, porosity, density absorption and related properties and swelling and slake- durability index properties. Int. J. Rock Mech. Min. Sci. **16**, 141–156. https://doi.org/10.1016/0148-9062(79)91453-0

Koca MY, Ozden G, Yavuz AB, Kincal C, Onargan T, Kucuk K (2006) Changes in the engineering properties of marble in fire-exposed columns. Int. J. Rock Mech. Min. Sci. **43**, 520–530. https://doi.org/10.1016/j.ijrmms.2005.09.007

Musso G, Cosentini RM, Foti S, Comina C, Capasso G (2015) Assessment of the structural representativeness of sample data sets for the mechanical characterization of deep formations. Geophysics **80**, D441–D457. https://doi.org/10.1190/GEO2014-0351.1

Schneider CA, Rasband WS, Eliceiri KW (2012) NIH Image to ImageJ: 25 years of image analysis. Nat. Methods. https://doi.org/10.1038/nmeth.2089

Talabani S, Boyd D, El Wazeer F, Al Arfi S (2000) Validity of archie equation in carbonate rocks, in: Society of Petroleum Engineers - Abu Dhabi International Petroleum Exhibition and Conference 2000, ADIPEC 2000. https://doi.org/10.2523/87302-ms

Vagnon F, Colombero C, Colombo F, Comina C, Ferrero AM, Mandrone G, Vinciguerra SC (2019) Effects of thermal treatment on physical and mechanical properties of Valdieri Marble - NW Italy. Int. J. Rock Mech. Min. Sci. **116**, 75–86. https://doi.org/10.1016/j.ijrmms.2019.03.006

Weydt LM, Bär K, Colombero C, Comina C, Deb P, Lepillier B, Mandrone G, Milsch H, Rochelle CA, Vagnon F, Sass I (2018) Outcrop analogue study to determine reservoir properties of the Los Humeros and Acoculco geothermal fields, Mexico. Adv. Geosci. **45**, 281–287. https://doi.org/10.5194/adgeo-45-281-2018

Zhao Y, Wan Z, Feng Z, Yang D, Zhang Y, Qu F (2012) Triaxial compression system for rock testing under high temperature and high pressure. Int. J. Rock Mech. Min. Sci. **52**, 132–138. https://doi.org/10.1016/j.ijrmms.2012.02.011

Table captions

Table 1: Percentage of mineral compounds and oxides retrieved from XRD and XRF analyses.

Table 2: Experimental instruments, international standards and main physical parameters.

Table 3: Summary of grain size distribution performed on microphotographs of the tested rocks.

Table 4: Summary of crack length results performed on microphotographs of the tested rocks.

List of Tables

Table 1: Percentage of mineral compounds and oxides retrieved from XRD and XRF analyses.

		RLM	GQ	VALDIERI	BRAZIL C	BRAZIL D	BRAZIL SJ
	Compound name	Concentration [%]					
XRD	Calcite	97.3	-	98	37.9	48.98	14.84
	Quartz	2.7	-	-	-	-	-
	Dolomite	-	100	2	42.58	42.46	73.33
	Forsterite	-	-	-	18	-	-
	Tremolite	-	-	-	1.47	-	2.02
	Wairauite	-	-	-	0.05	-	4.61
	Siderite	-	-	-	-	-	5.18
	Olivine	-	-	-	-	8.1	-
XRF	MgO	1.106	36.331	2.05	17.33	20.39	21.36
	CaO	96.529	62.495	97.02	78.84	67.37	76.45
	SiO_2	1.047	0.48	0.425	3.65	11.36	1.898
	AL_2O_3	0.356	0.118	0.18	-	0.54	-
	K_2O	0.33	0.195	-	-	-	-
	F	0.3	-	-	-	-	-
	CoO	-	0.149	-	0.014	-	0.006
	Fe_2O_3	0.131	-	0.13	0.05	0.26	0.17
	Others	0.21	0.233	0.195	0.104	0.0725	0.107

Table 2: Experimental instruments, international standards and main physical parameters.

Physical property	**International Standard**	**Test instrument**	**Technical parameters**
Porosity	ISRM. Suggested methods for determining water content, porosity, density, absorption and related properties and swelling and slake-durability index properties. 1977	Caliper Analytical balance	Resolution: 0.0002 m Resolution: 0.0001 kg
P- and S-wave velocity, VP and VS	ASTM D2845-08	Ultrasonic pulse generation and acquisition system (Pundit Lab, Proceq)	Two cylindrical 250-kHz tx-rx probes
ER measurement, ρ_{app_dry}	-	Syscal-Pro (Iris instruments) acquisition system	On-purpose built measuring quadrupole (Vagnon et al. 2019)
Heat treatment	-	Carbolite Temperature programmer Eurotherm 2416CG	Temperature range: 1100°C Heating rate: 0.06°C/s Resolution: 1°C
		XRF: S2 Ranger (Bruker Company)	

Table 3: Summary of grain size distribution performed on microphotographs of the tested rocks.

Set	T [°C]	D50 [mm]	CU [-]
RLM	20	0.0227	5.05
	600	0.019	5.04
VALDIERI	20	0.009	2.20
	600	0.009	3.26
GQ	20	0.0045	3.65
	600	0.004	5.80
BRAZIL C	20	0.0227	6.96
	600	0.01	4.44
BRAZIL D	20	0.019	2.61
	600	0.01	4.22
BRAZIL SJ	20	0.0102	3.62
	600	0.0087	2.27

Table 4: Summary of crack length results performed on microphotographs of the tested rocks.

Set	T [°C]	Crack length [mm]			Crack density [1/mm]
		Min	Max	Median	
RLM	20	0.003	0.219	0.009	32.376
	600	0.003	0.898	0.012	42.015
VALDIERI	20	0.003	0.303	0.020	28.896
	600	0.003	0.258	0.024	37.444
GQ	20	0.001	0.090	0.008	47.362
	600	0.001	0.136	0.008	49.994
BRAZIL C	20	0.003	0.672	0.029	12.195
	600	0.003	0.553	0.036	16.182
BRAZIL D	20	0.003	0.603	0.022	14.120
	600	0.003	0.739	0.023	15.560
BRAZIL SJ	20	0.003	0.552	0.021	12.444
	600	0.003	0.718	0.022	15.951

Figure captions

Figure 1: Location of the four sampling areas and pictures of the different sets of specimens.

Figure 2: Relationship between porosity (a), P-wave velocity (b), S-wave velocity (c) and formation factor (d) and temperature for the studied samples. All the data are associated to their standard deviations: where not visible, the length of the error bars is lower than the marker size.

Figure 3: Relationship between formation factor and porosity for the studied samples. All the data are associated to their standard deviations: where not visible, the length of the error bars is lower than the marker size.

Figure 4: Relationship between P-wave (a) and S-wave (b) velocity and porosity for the studied samples.

Figure 5: Optical microscope observations of specimens at 20°C (left column) and at 600°C (right column).

Figure 6: Cumulative (a) and derivative (b to g for each sample) grain size distributions of microphotographs at room temperature (continuous lines) and at 600°C (dashed lines).

Figure 7: Frequency (column bars) and cumulative (dashed lines) distribution of crack length for each sample at 20°C (blue) and at 600°C (orange).

Figure 8: Relationship between the induced damage index for a) porosity, b) formation factor, c) P- and d) S-wave velocity and temperature.

List of Figures

Figure 1: Location of the four sampling areas and pictures of the different sets of specimens.

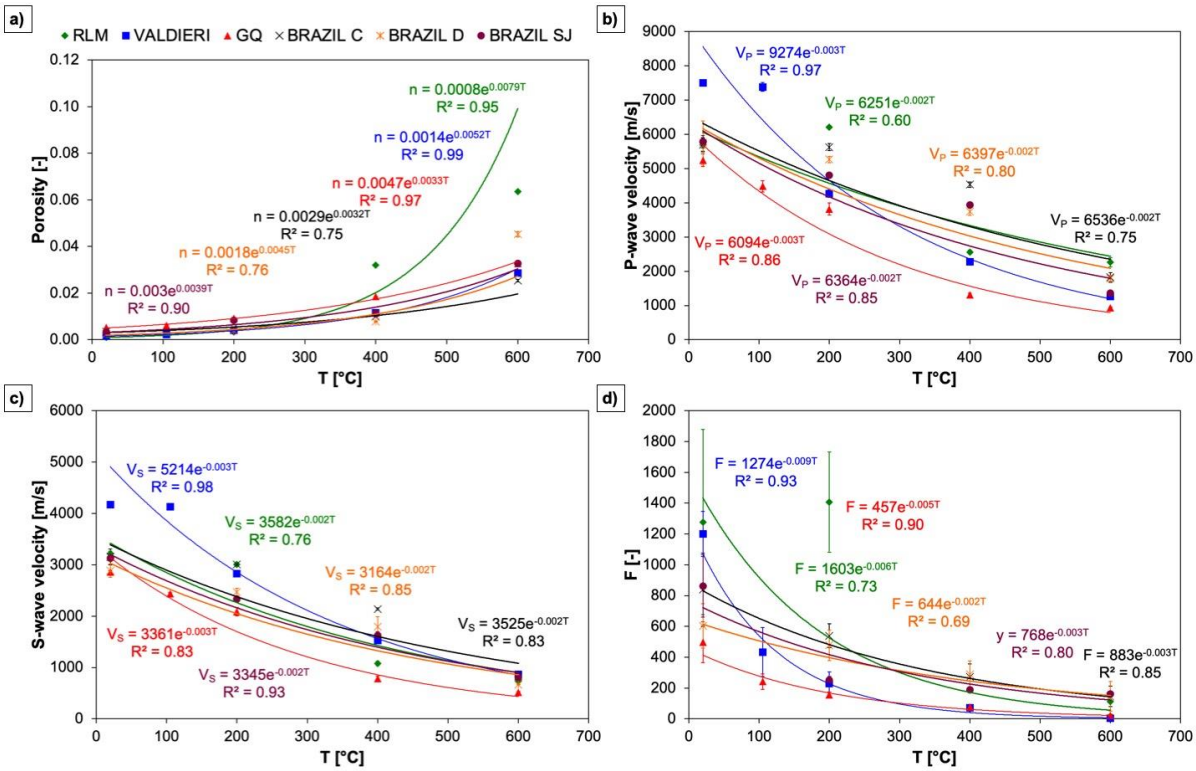

Figure 2: Relationship between porosity (a), P-wave velocity (b), S-wave velocity (c) and formation factor (d) and temperature for the studied samples.

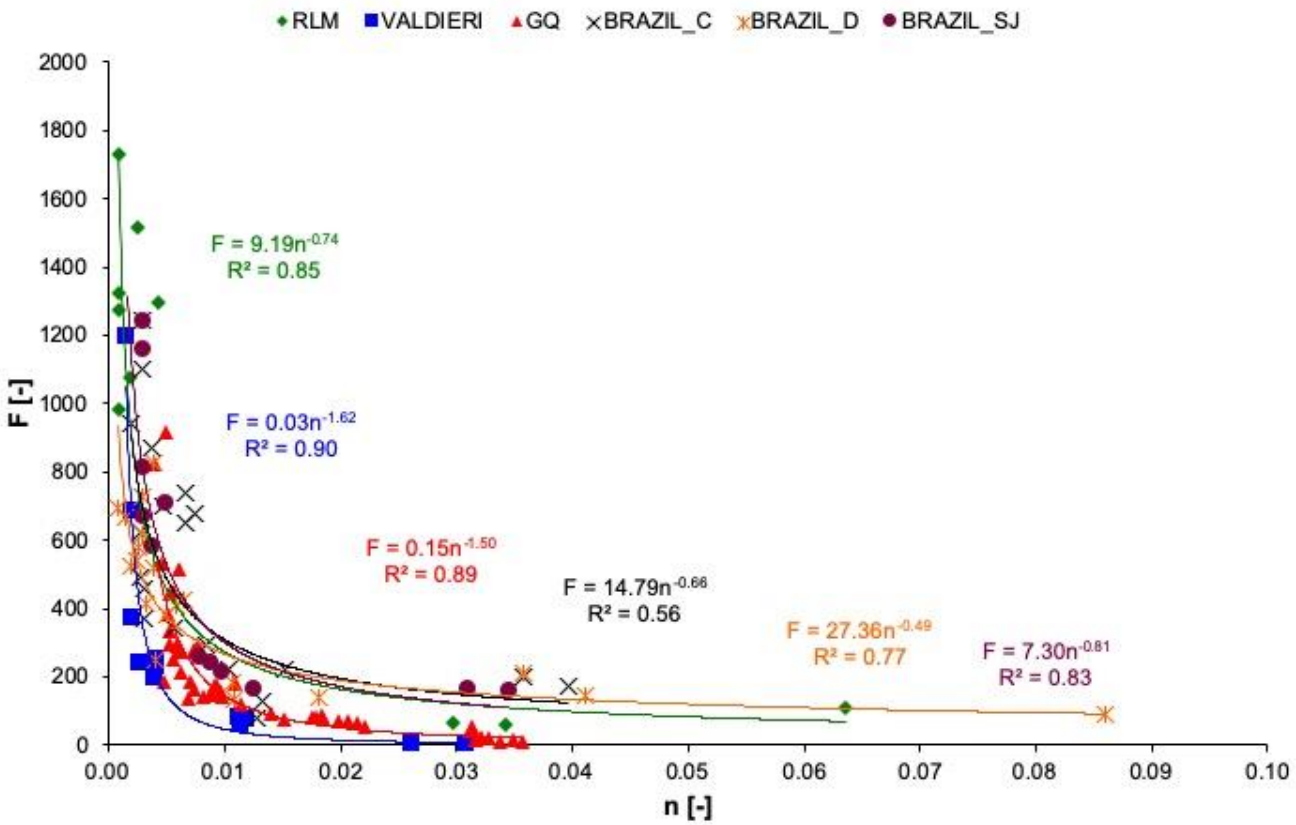

Figure 3: Relationship between formation factor and porosity for the studied samples.

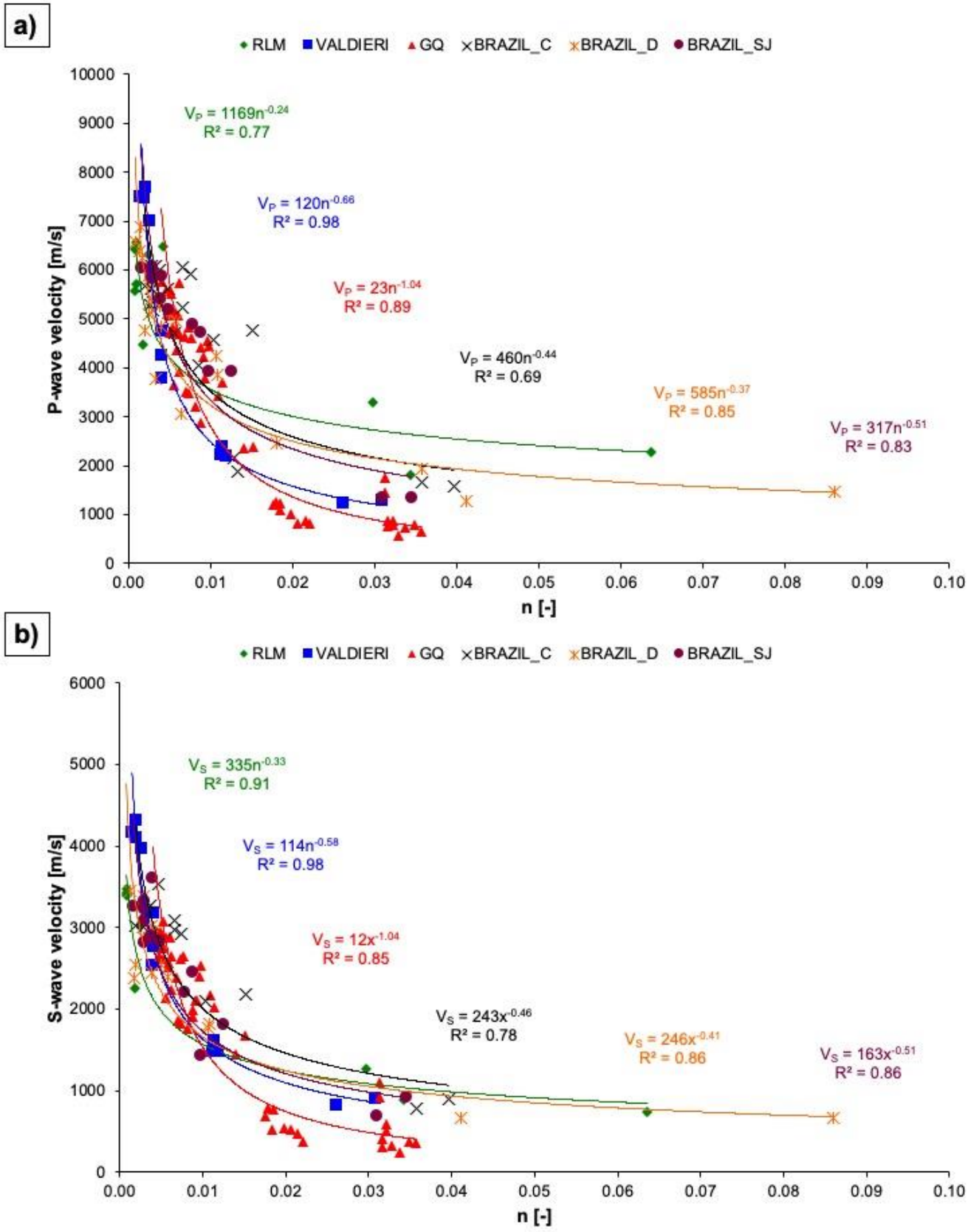

Figure 4: Relationship between P-wave (a) and S-wave (b) velocity and porosity for the studied samples.

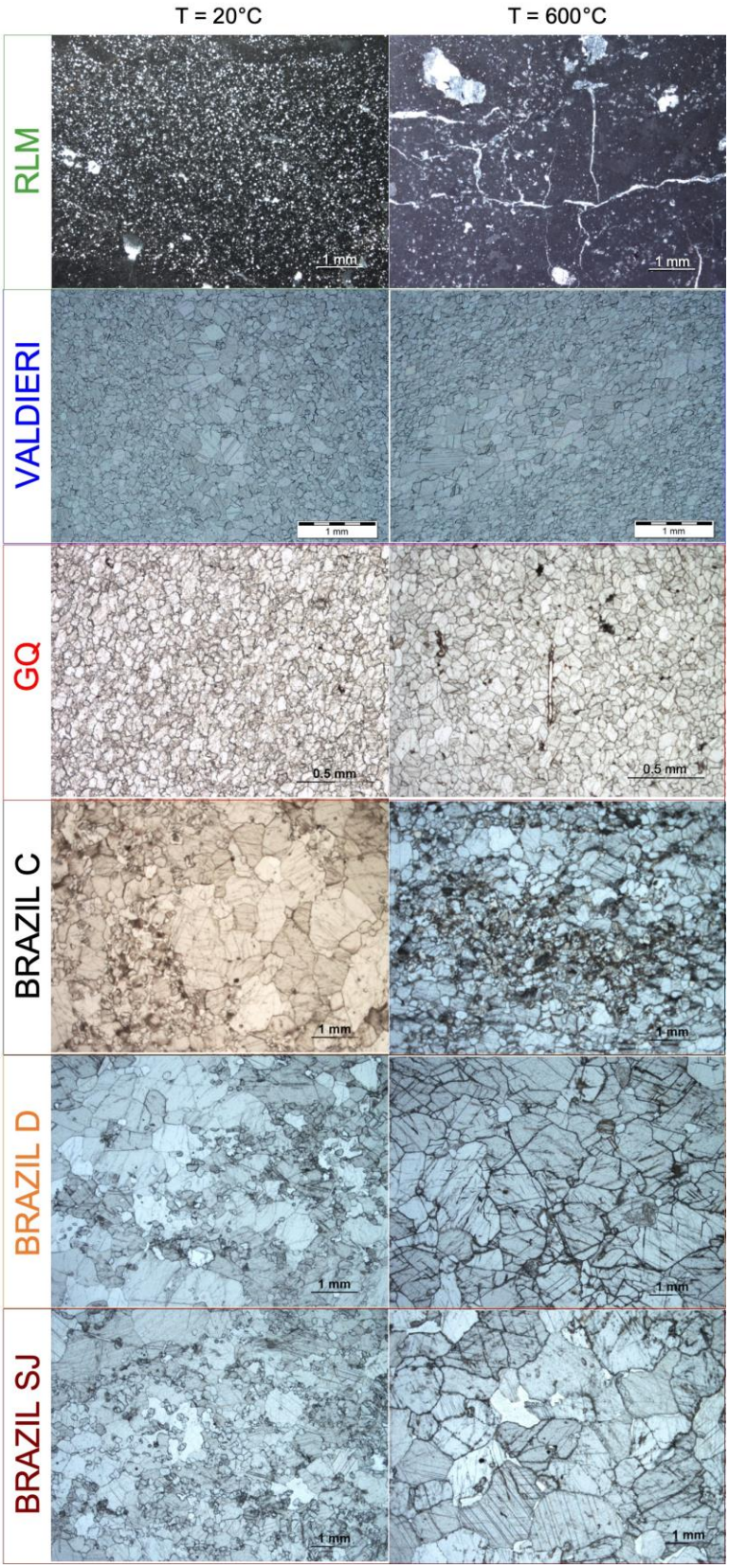

Figure 5: Optical microscope observations of specimens at 20°C (left column) and at 600°C (right column).

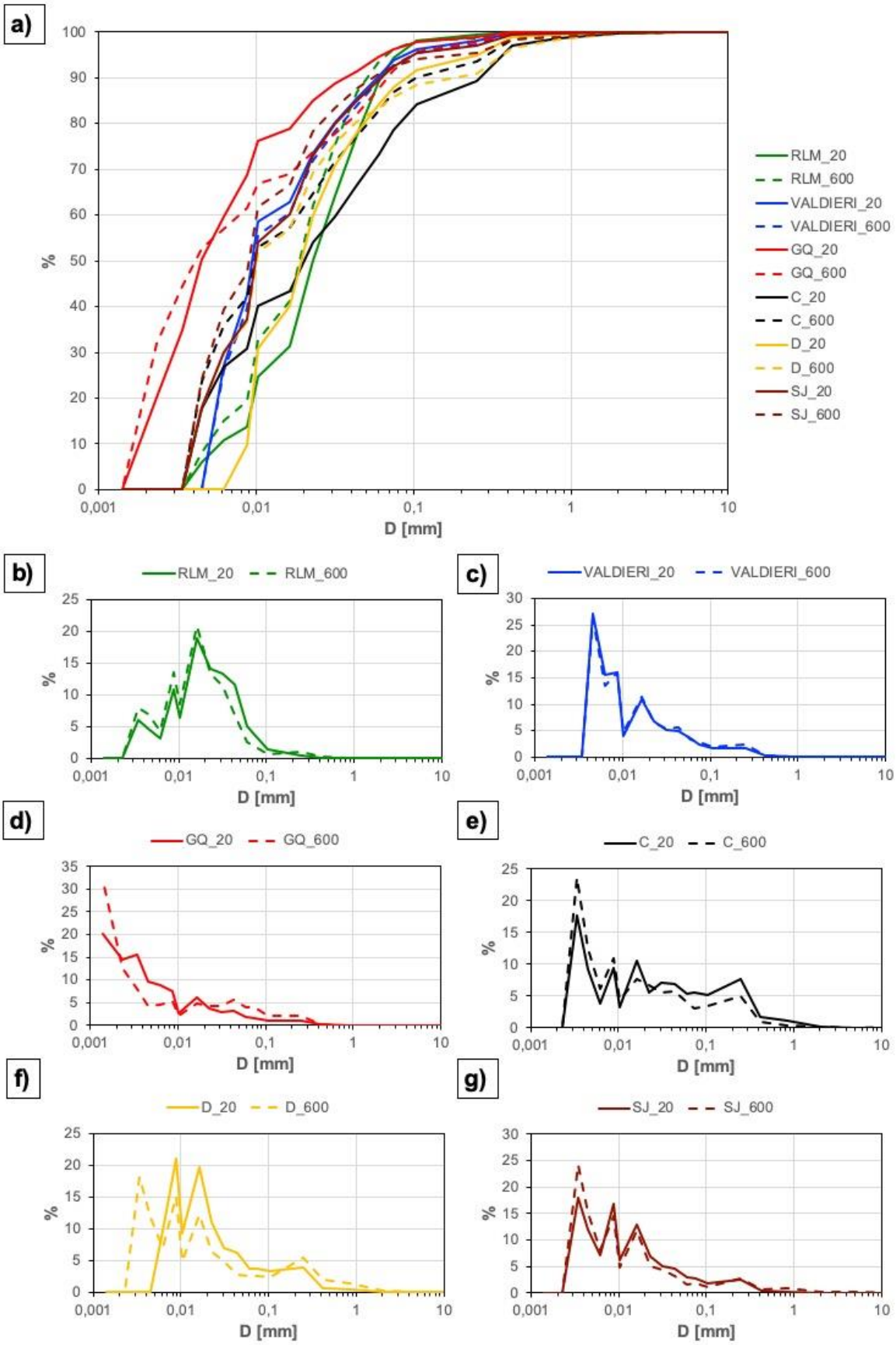

Figure 6: Cumulative (a) and derivative (b to g for each sample) grain size distributions of microphotographs at room temperature (continuous lines) and at 600°C (dashed lines).

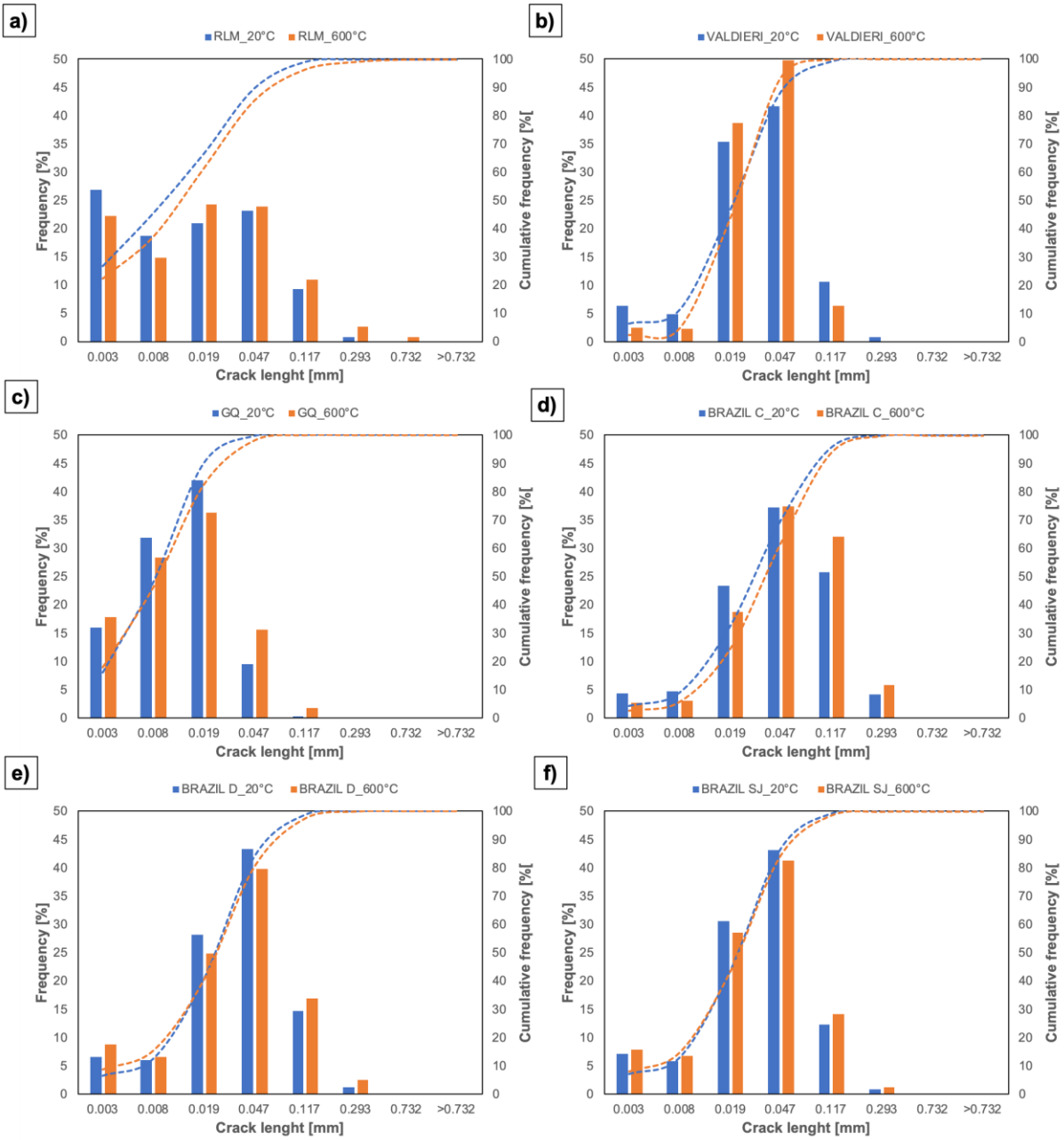

Figure 7: Frequency (column bars) and cumulative (dashed lines) distribution of crack length for each sample at 20°C (blue) and at 600°C (orange).

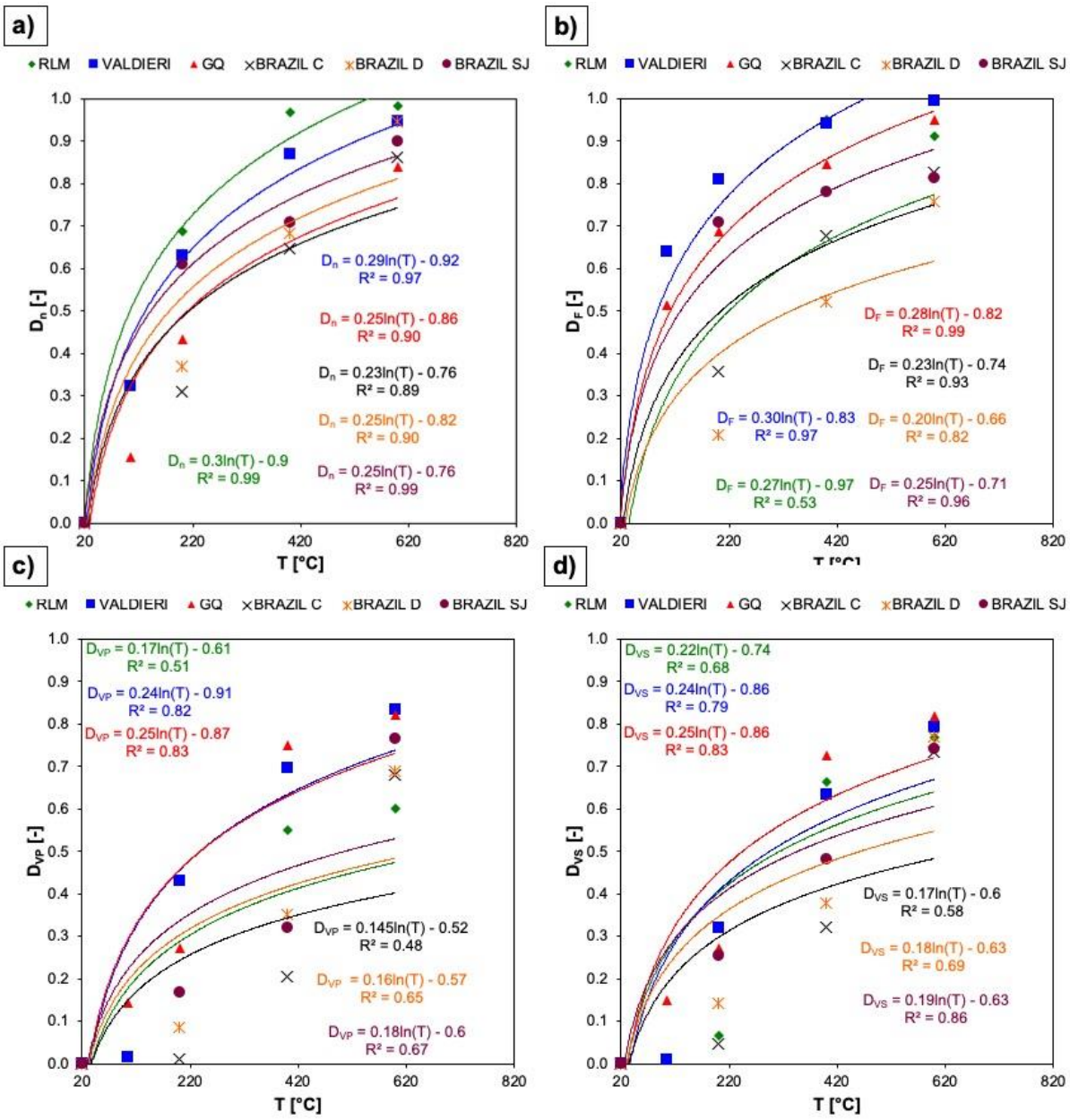

Figure 8: Relationship between the induced damage index for a) porosity, b) formation factor, c) P- and d) S-wave velocity and temperature.